

CRISPR/Cas9 and Chlorophyll Coordination Micelles for Cancer Treatment by Genome Editing and Photodynamic Therapy

Chen Zhang, Xiaojie Wang, Gengqi Liu, He Ren, Jingang Liu, Zhen Jiang, and Yumiao Zhang*

CRISPR/Cas9-based gene therapy and photodynamic therapy both show promise for cancer treatment but still have their drawbacks limited by tumor microenvironment and long treatment duration. Herein, CRISPR/Cas9 genome editing and photodynamic strategy for a synergistic anti-tumor therapeutic modality is merged. Chlorophyll (Chl) extracted from natural green vegetables is encapsulated in Pluronic F127 (F127) micelles and Histidine-tagged Cas9 can be effectively chelated onto micelles via metal coordination by simple incubation, affording Cas9-Chl@F127 micelles. Mg²⁺ acts as an enzyme cofactor to correlatively enhance Cas9 gene-editing activity. Upon laser irradiation, Chl as an effective photosensitizer generates reactive oxygen species (ROS) to kill tumor cells. Meanwhile, CRISPR/Cas9, mediated by dual deliberately designed gRNAs of APE1 and NRF2, can reprogram the tumor microenvironment by increasing the intracellular oxygen accumulation and impairing the oxidative defense system of tumor cells. Cas9-Chl@F127 micelles can responsively release Cas9 in the presence of abundant ATP or low pH in tumor cells. In a murine tumor model, Cas9-Chl@F127 complexed with dual gRNAs including APE1 and NRF2 significantly inhibits the tumor growth. Taken together, Cas9-Chl@F127 micelles, representing the first Chl-based green biomaterial for the delivery of Cas9, show great promise for the synergistic anti-tumor treatment by PDT and gene editing.

undesirable gene modifications and toxicity to normal cells.^[6,7] To mitigate this issue and augment the therapeutic efficacy, a variety of responsive biomaterials have been developed to release Cas9, triggered by stimuli such as glutathione, light and ultrasound.^[8–16] However, some of these methods involve chemical modification or protein engineering of Cas9, which might alter Cas9 conformation and impair the endonuclease activity. In addition, some chemical byproducts after triggered release can potentially cause cytotoxicity.^[17] Chlorophyll, naturally existing in green plants, has a macrocycle structure with magnesium ions (Mg²⁺) chelated in the center, which can also coordinate with Histidine (His)-tagged Cas9, but chlorophyll-based biomaterials have rarely been used for Cas9 delivery to our knowledge. Importantly, Mg coordinated with His-tagged Cas9 can be de-chelated to triggered release Cas9 in the presence of abundant ATP or acidic conditions in the tumor microenvironment, without altering the structure of Cas9 or impairing

the function of Cas9. In addition, Cas9 could be effectively coordinated to chlorophyll by simply admixing and incubation. This approach has advantages of facile preparation and good stability, compared with physical entrapment and covalent conjugation.^[18–20]

For the cancer treatment, the gene editing efficiency in cancer cells by CRISPR/Cas9 could be enhanced in combination with other therapies.^[21] Photodynamic therapy (PDT) is a clinical-stage tumor ablation paradigm combining photosensitizer with light irradiation, but overdosed photosensitizers accumulated in the body could cause phototoxicity.^[22,23] Chlorophyll can act as a “green” photosensitizer used in PDT and the combination of PDT and CRISPR/Cas9 could achieve better and safer therapeutic effect. Spatiotemporal regulation of CRISPR/Cas9 was realized by control of light, resulting in reduced off-target effect.^[24,25] The addition of CRISPR/Cas9 significantly reduces the dose of photosensitizer and corresponding phototoxicity. In addition, rapid proliferation of tumor cell leads to hypoxic tumor microenvironment, which hampers the generation of reactive oxygen species (ROS) and results in suboptimal

1. Introduction

The cluster regularly interspaced short palindromic repeat (CRISPR)-associated protein 9 (Cas9)-based therapeutic genome editing has shown great promise to cure various genetic diseases.^[1–3] Mediated by guide RNA (gRNA) to edit target genes, CRISPR/Cas9 system has the advantages of high precision and specificity, low cost, and safety.^[4,5] However, CRISPR/Cas9 still faces some challenges such as off-target effect to cause

C. Zhang, X. Wang, G. Liu, H. Ren, J. Liu, Z. Jiang, Y. Zhang
School of Chemical Engineering and Technology
Key Laboratory of Systems Bioengineering (Ministry of Education)
Frontiers Science Center for Synthetic Biology (Ministry of Education)
Tianjin University
Tianjin 300350, P. R. China
E-mail: ymzhang88@tju.edu.cn

 The ORCID identification number(s) for the author(s) of this article can be found under <https://doi.org/10.1002/smll.202206981>.

DOI: 10.1002/smll.202206981

PDT outcomes.^[26,27] CRISPR/Cas9 can reprogram the tumor microenvironment and enhance the PDT effect. For example, apurinic/aprimidinic endonuclease 1 (APE1) protein is associated with mitochondrial functions and the downregulation of APE1 by CRISPR/Cas9 results in increased accumulation of oxygen.^[28,29] In addition, nuclear factor-erythroid 2-related factor 2 (NRF2) act as a self-defense system in tumor cell to avoid the oxidative damage caused by ROS. Low expression of NRF2 inhibits tumor cell repair process and leads to enhanced anti-tumor effect.^[30,31] On the other hand, the gene editing efficacy of CRISPR/Cas9 system is also greatly dependent on catalytic activity of Cas9. And it has been shown that many metal ions such as Pb²⁺, Zn²⁺, Mn²⁺, and Mg²⁺ can act as cofactors to significantly increase the activity of various enzymes.^[32,33] Mg²⁺ can enhance the endonuclease activity of Cas9 by altering Cas9 nucleophilicity.^[34,35] Therefore, the naturally existing chlorophyll containing abundant Mg²⁺ can provide for the basis of Cas9 scaffolding structures, act as a photosensitizer for PDT and also augment the endonuclease activity of Cas9.

Taking the aforementioned points into consideration, we designed a synergistic anti-tumor strategy based on photodynamic therapy and gene editing. Chlorophyll extracted from chlorella was first encapsulated in Pluronic F127 (F127) micelles, followed by simply admixing Chl@F127 and His-tagged Cas9 to chelate Cas9 onto micelles to make Cas9-Chl@F127. Upon laser irradiation, Chl as an effective photosensitizer could generate ROS to kill cancer cells. Furthermore, once Cas9-Chl@F127 micelles are up taken in tumor cells, Cas9 could be released in response to intracellular abundant ATP and acidic environment in lysosomes. Mediated by dual deliberately designed gRNAs, Cas9-Chl@F127 enhanced intracellular oxygen accumulation and impaired the defense system of cancer cells, by knockout of APE1 and NRF2 genes, leading to amplified PDT efficacy. In addition, Mg²⁺ in the center of chlorophyll serves as a cofactor to greatly augment gene editing activity of Cas9 (Scheme 1).

2. Experimental Section

2.1. Extraction of Chlorophyll

5 g chlorella was dissolved in 150 mL 90% ethanol aqueous solution and stirred in the dark for 3 h. After being centrifuged at 3400 rpm for 15 min, the supernatant was filtered through 0.22 μm membrane, then 48 mL dioxane and 48 mL water was added, respectively. Then the solution was stored at -20 °C overnight. Precipitate was collected through 0.22 μm membrane, washed with water three times, and then dried at 37 °C overnight. 15 mL 1 M hydrochloric acid was added to the 150 mL chlorophyll ethanol solution, and Pheophytin (Pheo) could be obtained according to the abovementioned method.^[47] Mass spectrum of Chl and pheo are shown in Figure S2, Supporting Information.

2.2. Preparation and Characterization of Cas9 and RNP

Cas9 protein was obtained according to the authors' previous published method. Briefly, the *Escherichia coli* BL21 (DE3) pLys was used as a host to express the plasmid pET-28b-Cas9

for the generation of Cas9 protein. First, a single colony was inoculated and cultured overnight in Luria–Bertani (LB) broth containing 50 μg mL⁻¹ kanamycin at 37 °C. Then the seed solution was diluted by 1:100 into LB medium and then subject to shaking at 37 °C until OD600 was around 0.6. Next, isopropyl β-D-thiogalactoside (IPTG) at a final concentration of 0.2 mM was added for induction of Cas9 and maintained at 18 °C. After 14 h, the bacteria were collected, re-suspended in the binding buffer (10 mM Tris, 50 mM NaH₂PO₄, 300 mM NaCl, 20 mM imidazole), and subsequently subjected to sonication. After centrifugation, the resulting supernatant was purified by HisTrap (GE) column with elution buffer (10 mM Tris, 50 mM NaH₂PO₄, 300 mM NaCl, 250 mM imidazole). Finally, the collected Cas9 were collected and concentrated by 10 kDa ultra-centrifugal filtration devices. BMCA protein assay kit was used to quantify the Cas9 content. The final product of Cas 9 protein was stored in storage buffer (50 mM Tris, 200 mM KCl, 0.1 mM EDTA, 10% glycerol) at -80 °C. The endonuclease activity of purified Cas9 was determined by digesting the plasmids and DNA fragment. Cas 9 and sgRNA (molar ratio of 1:1) were mixed and incubated at room temperature for 10 min to form Cas9 protein/guide RNA ribonucleoprotein complexes (Cas9 RNP).

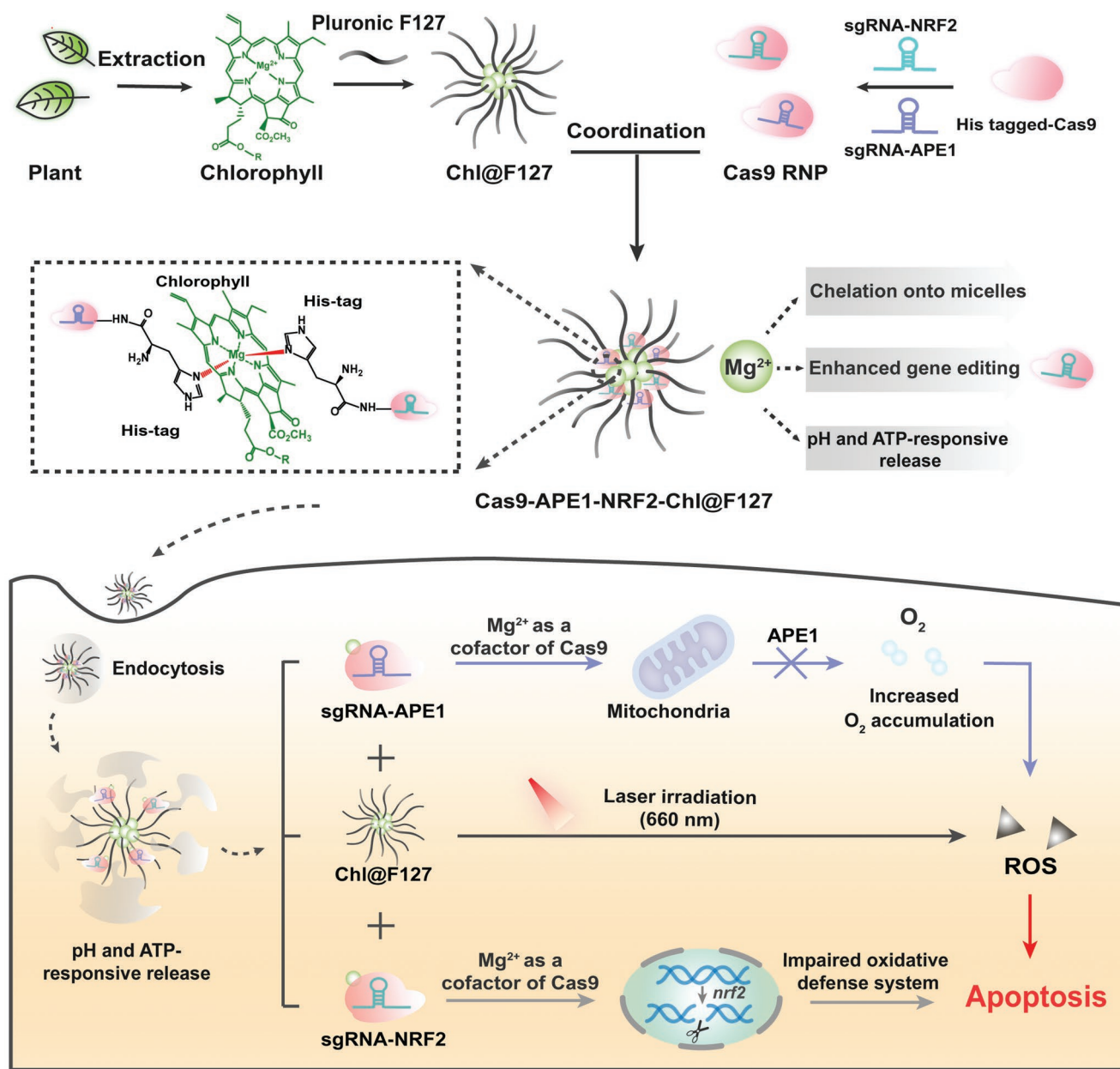
2.3. Preparation and Characterization of Cas9-Chl@F127

1 mg chlorophyll dissolved in 1 mL tetrahydrofuran (THF) was added to 10 mL 10% v/v Pluronic F127 aqueous solution, and then sonicated for 15 min, followed by washing by ultrafiltration with 100 kDa molecular weight cut off (MWCO) tubes for three times. 1 mg Pheophytin dissolved in 1 mL THF was added to 10 mL 10% v/v Pluronic F127 aqueous solution, and ultrasonically oscillated for 15 min, then zinc chloride in 0.1 M sodium acetate aqueous solution was added at a molar ratio of 1 (Pheo):100 (Zn), the solution was stirred overnight and washed three times with 100 kDa ultrafiltration tubes. Chl/Pheo content in micelles was determined by UV–VIS spectrophotometer.

Cas9-Chl@F127 and Cas9-Zn-Pheo@F127 were obtained by adding Cas9 to a Chl/Pheo micelle solution at the molar ratio of 1:10, incubation overnight. The size of all samples was measured by Zetasizer instrument (Malvern, England) in aqueous solutions. Transmission electron microscopic (TEM) images were collected by a JEM-2100F system (JEOL, Japan).

In order to make amine-modified F127, the hydroxyl group of Pluronic F127 was first activated by carbonyldiimidazole and then reacted with 1,2-ethanediamine. The reactant molar ratio was 1 to 1 and product was collected by reprecipitation in cold ethyl ether for each step. Chl and Pheo in amine-modified F127 micelles was made similarly as described above. Micelles were labeled with Cy5 in dimethyl sulfoxide (DMSO) overnight, and Cas9 protein was labeled by Cy3 overnight. The excess Cy5 and Cy3 were removed by dialysis, and the Chl/Pheo-Cy5 micelles were mixed with Cas9-Cy3 at a molar ratio of 1:1 overnight. UV–VIS spectrophotometer was used to analyze the results. The fluorescence at 550–700 nm was measured, and the excitation wavelength was chosen at 528 nm.

Cas9 were fluorescently labelled with fluorescein isothiocyanate (FITC), and then Cas9-Chl@Pluronic and Cas9-Zn-Pheo@Pluronic micelles of Pluronic F127, F68 and



Scheme 1. Illustration of micellar chlorophyll coordinating CRISPR/Cas9 for synergistic tumor treatment by genome editing and photodynamic therapy. RNP: Cas9 protein/guide RNA ribonucleoprotein complexes.

F108 were prepared according to the above method. After overnight dialysis, the fluorescence values of all samples were measured and the loading efficiency were calculated (Figure S4, Supporting Information). FITC-labeled Cas9-Chl@F127 and Cas9-Zn-Pheo@F127 were prepared according to the above method and incubated in 10% v/v FBS and PBS at 37 °C, and 50 μ L samples were taken every 2 h and the fluorescence values were measured. excitation: 428 nm, emission: 525 nm.

2.4. Evaluation of 1O_2 Generation In Vitro

1'3-diphenylisobenzofuran (DPBF) dissolved in DMSO was added to the Cas9-Chl@F127 and Cas9-Zn-Pheo@F127

solutions at a final concentration of 10 μ M, then the samples were irradiated by a 660 nm laser with fluence rate of 0.1 W cm^{-2} for 15 min, and the absorption spectra at 250–500 nm were measured. Electron spin resonance (ESR) spectrometer was used to further confirm the generation of $\cdot OH$ unequivocally with 2,2,6,6-tetramethylpiperidine (TEMP) as a capturing agent of hydroxyl radicals.

2.5. Validation of the Effect of Metal Ions on the Activity of Cas9

1 μ L sgRNA (0.25 μ g μ L $^{-1}$) and 1 μ L Cas9 (1 mg mL^{-1}) were mixed for 10 min, then 2 μ L EGFP DNA fragment (5785 μ g μ L $^{-1}$),

5 μ L water, 1 μ L buffer (100 mM NaCl, 50 mM Tris-HCl, and 1 mM DTT), and 1 μ L MgCl₂, MnCl₂, ZnCl₂, NiCl₂, CuCl₂, FeCl₂, CoCl₂ and CaCl₂ aqueous solution (100 mM) were added. The sgRNA were purchased from GENEWIZ company, EGFP sgRNA sequence: 5'-ccggcaagctgccctgtccc-3'. Scaffold sequence: 5'-gttttagagctagaatagcaagtaa aataaggctagctccgttatcaactgaaaa-gtgg-3'. The EGFP DNA fragment was a 738 bp dsDNA fragment containing guide RNA targeted sequences amplified by PCR. Specific sequence: 5-ataaggatccgatggtagcaagggcgaggagctgttca ccgggtgtgcccactctggctgagctggagcggcgcgacgtaaacggccacaagttcagcgt-gtccggcgagggcgagggcgatgccacactcggcaagctgacctgaagttcatctg-caccaccggcaagctgccctgcccctgcccaccctctgaccaccctgacctcggcgt-gcagtgcttcagcggctaccccgaccacatgaagcagcagcacttctcaagtcggccatgc-cggaaggctacgtccaggagcgcaccatcttcaaggacgacggcaactacaagacc-cgcggcaggtgaagttcagggcgacacctggtgaaccgcatcgagctgaagggcatc-gacttcaaggagcggcaacatcctggggcacaagctggagtacaactacaacagc-cacaacgtctatatcatggccgacaagcagaagaacggcatcaaggtgaactcaagatc-cgccacaacatcgaggagcggcagcgtgacgctcggaccactaccagcagaacacc-cacatcgggcagcggcccctgctgctgcccgacaaccactacgtgacccagtcggccct-gagcaaacgcccacagagaagcgcgatcacatggctctgctggagttcgtgaccgc-cgcccggatcactctggcagcagcgtgtaagaagctgat-3. All samples were placed at 37 °C for 2 h, then 1 μ L protease was added. The samples were analyzed by electrophoresis in 2% m/v agarose gel in Figure S1, Supporting Information.

0.35 μ L sgRNA (0.25 μ g μ L⁻¹) and 0.35 μ L Cas9 (1 mg mL⁻¹) were mixed for 10 min, then 1.4 μ L EGFP DNA fragment (57.85 μ g μ L⁻¹), 3.5 μ L water, 0.7 μ L buffer (100 mM NaCl, 50 mM Tris-HCl and 1 mM DTT) and 0.7 μ L MgCl₂ aqueous solution was added. All samples were placed at 37 °C for 0.5 h, then 1 μ L protease was added. The samples were analyzed by electrophoresis in 2% m/v agarose gel in Figure 1a.

2.6. Release Kinetics of Cas9 Triggered by ATP and pH

The pH of Cas9-Chl@F127 micelles aqueous solution were adjusted to 3, 4, 5, 6 and 7.4 by hydrochloric acid, and the ATP content of the Cas9-Chl@F127 micelles aqueous solution was adjusted to 0, 2, 5 and 10 mM. After shaking overnight at 25 °C, the absorption spectra of all samples were measured, and the data were recorded by taking pictures and the polarity were also analyzed by thin layer chromatography with elution solution of hexane:ethyl acetate = 7:3.

300 μ L Cas9-Chl@F127 micelle aqueous solution (240 μ g Cas9) was put in a dialysis bag (molecular weight cut off [MWCO]: 300 000 Dalton), and placed in 150 mL different solutions including 0.1 mM ATP, 10 mM ATP, pH = 5.5, pH = 7.4, 0.1 mM ATP+pH = 7.4, and 10 mM ATP+pH = 5.5 PBS aqueous solution, respectively. 20 μ L samples were taken out at 0, 0.25, 0.5, 1, 2, 3, 4, 6, 8, 10, and 12 h and the protein concentration was performed by BCA protein assay kits.

The Cas9-Chl@F127 solutions were immersed in 10 mM ATP, pH = 5.5, and 10 mM ATP+pH = 5.5 PBS solution overnight. All samples were analyzed, followed by the measurement of size and 12% sodium dodecyl sulfate polyacrylamide gel electrophoresis (SDS-PAGE), and the cleavage activity of Cas9 protein were also assessed according to the above-mentioned method.

2.7. Cellular Uptake

Human pulmonary carcinoma A549 cells were cultured in The Roswell Park Memorial Institute 1640 (RPMI-1640) supplemented with 10% v/v FBS and 1% v/v penicillin-streptomycin at 37 °C in a humid atmosphere containing 5% CO₂. 5 \times 10⁴ cells/well were seeded in 24-well plates and cultured overnight. FITC was used as an indicator to monitor the internalization process, FITC labelled Cas9-Chl@F127 (7 μ g Cas9) was added to each well at 0, 2, 4, 6, 8, 12 and 24 h, respectively. The cells were washed with PBS and the nucleus was stained with 200 μ L 2-(4-amidinophenyl)-6-indolecarbamide dihydrochloride (DAPI) for 15 min. After the fluorescence images were acquired from microscope, the radio immunoprecipitation assay (RIPA) lysis buffer was added and incubated for 2 h, subsequently, the fluorescence values were measured using spectrometer.

As for the lysosomal escape experiment, 5 \times 10⁴ cells/well were seeded in 24-well plates and cultured overnight, Cas9-FITC (14 μ g Cas9), FITC-Cas9-Zn-Pheo@F127 (14 μ g Cas9) and FITC-Cas9-Chl@F127 (14 μ g Cas9) were added, respectively. After culturing for 8 h, the cells were washed with PBS, and the cell nuclei and lysosomes were stained by DAPI and LysoTracker Red, respectively, then the images were taken by microscope.

1 \times 10⁵ A549 cells/well were seeded in 96-well plates and cultured overnight, then the cells were treated by macropinosytosis-mediated endocytosis inhibitor amiloride (3.6 mg mL⁻¹), caveolae-dependent endocytosis inhibitor methyl- β -cyclodextrin (M β CD) (75 mg mL⁻¹) or 4 °C. Then RIPA lysis buffer was added and incubated for 2 h, subsequently, the fluorescence values were measured by spectrometer.

2.8. Determination of Intracellular ROS Generation

5 \times 10⁴ cells/well were seeded in 24-well plates and cultured overnight, Cas9 (14 μ g Cas9), Cas9-Zn-Pheo@F127 (14 μ g Cas9), Cas9-Chl@F127 (14 μ g Cas9), Chl@F127, Cas9-APE1-Chl@F127 (14 μ g Cas9), Cas9-NRF2-Chl@F127, and Cas9-APE1-NRF2-Chl@F127 (14 μ g Cas9) was added and incubated for 8 h. Then the cells were washed with PBS, and 2',7'-dichlorodihydrofluorescein diacetates (DCFH-DA) were added to a final concentration of 20 μ M. After irradiating with laser for 3 min, the ROS production were analyzed by microscope. The content of intracellular ATP was detected by ATP Assay Kit according to the manufacturer's instructions.

2.9. EGFP Gene Disruption Assay in A549 Cells

A549 cells (1 \times 10⁴ cells/well) EGFP were seeded in 96-well plates and cultured overnight, then Cas9 (1.75 μ g Cas9), Cas9-Zn-Pheo@F127 (1.75 μ g Cas9) and Cas9-Chl@F127 (1.75 μ g Cas9) were added, after culturing 24 h, the fluorescence intensity of cells was detected by microscope. Similarly, 2.5 \times 10⁵ A549 cells EGFP were seeded in each well of 6-well plates and cultured overnight. Cas9 (24 μ g Cas9), Cas9-Zn-Pheo@F127 (24 μ g Cas9) and Cas9-Chl@F127 (24 μ g Cas9) were added to

culture for 24 h, thereafter the expression of green fluorescent protein was determined by flow cytometry.

2.10. Determination of Intracellular Mg²⁺ Content

5 × 10⁵ cells were seeded in each well of a 6-well plate, Cas9-Chl@F127 (24 μg Cas9) were added and cultured for 72 h. After washing with PBS, trypsin was added to digest cells, and cells were resuspended in PBS and counted. Finally, the cells were treated with aqua regia (3 mL hydrochloric acid and 1 mL nitric acid) and measured by inductive coupled plasma emission spectrometer.

2.11. Cell Viability Assay

A549/NIH-3T3 (mouse embryonic fibroblast cells) was cultured in 96-well plates at a density of 2 × 10⁴ cells/well. Samples were added and cultured for 12 h, then each well was irradiated by a 660 nm laser with fluence rates 0.1 W cm⁻² for 5 min. After culturing for 48 h, Cell Counting Kit-8 (CCK-8 kit) solution was added and cultured for 4 h, the absorbance at 450 nm were measured. The samples were prepared and stained with calcein-AM and propidium (PI) according to the manufacturer's instructions, the results were recorded with optical microscope.

YF488-Annexin V/PI kit was used to evaluate A549 cells apoptosis. A549 cells (1 × 10⁵ cells/well) was cultured in a 6-well plate overnight, and samples were added and cultured for 12 h, then each sample was irradiated by a 660 nm laser with fluence rates 0.1 W cm⁻² for 5 min. After culturing for 48 h, the cells were stained by YF488-Annexin and propidium according to the manufacturer's instructions followed by the analysis by flow cytometry.

2.12. Immunofluorescence Analysis

A549 cells were seeded at a density of 5 × 10⁴ cells/well in 24-well plates and cultured overnight. The sample were added and incubated for 12 h, then each well was irradiated by a 660 nm laser with fluence rates 0.1 W cm⁻² for 5 min. After the cells were incubated for 48 h, glutaraldehyde was added and incubated for 20 min, 0.2% v/v Triton-X-100 solution were added and incubated for 15 min, 5% m/v BSA solution were added and incubated for 2 h, then rabbit anti-EGFP were added and incubated overnight. Finally, goat anti-rabbit IgG Alexa Fluor 488 were added and incubated overnight for 2 h, nuclei were stained with DAPI for 15 min, the results were recorded with a microscope.

2.13. Western Blot

5 × 10⁵ cells were seeded in 6-well plates, and Cas9(24 μg Cas9), Cas9-APE1-NRF2-Zn-Pheo@F127 (24 μg Cas9) and Cas9-APE1-NRF2-Chl@F127 (24 μg Cas9) were added and cultured for 12 h, after irradiating by a 660 nm laser with fluence rate of 0.1 W cm⁻² for 5 min, the cells were then cultured for 72 h.

After washing with PBS, RIPA lysis buffer was added in each well, the lysate was centrifuged at 12 000 rpm for 15 min at 4 °C. The protein in supernatant was separated by 10% m/v SDS polyacrylamide gel electrophoresis. Then samples were transferred to the PVDF membrane, and the transferred PVDF membrane was washed three times with Tris Buffered Saline with Tween 20 (TBST) solution for 10 min at 30 rpm. The transferred PVDF membrane were incubated in 5% w/v milk solution for 2 h, then washed three times with TBST solution. Rabbit anti-APE1 and rabbit anti-NRF2 diluted in 5% w/v milk solution were added and the samples were placed at 4 °C overnight, then the sample were washed three times with TBST solutions, goat anti-mouse IgG HRP antibody diluted in 5% w/v milk solution were added and cultured at 30 rpm for 2 h, GAPDH was chosen as control.

2.14. In Vivo Tumor Suppression

Female Balb/c nude mice (five weeks old, 14 g) were purchased from Charles River Beijing Co., Ltd (Beijing, China). Animal experiments were performed in accordance with Tianjin University Institutional Animal Care and Use Committee.

A549 cells suspended in PBS were inoculated in mouse subcutaneously to establish tumor models (1 × 10⁸ cells per mouse). Tumor-bearing mice (tumor size of 50 mm³) were randomly divided to six groups (four mice per group) to study the effects of PBS, Chl@F127, Cas9-APE1-Chl@F127, Cas9-NRF2-Chl@F127, Cas9-APE1-Zn-Pheo@F127, and Cas9-APE1-NRF2-Chl@F127 on tumor progression. 12.5 μg Cas9 in the various forms above was injected per mouse intravenously every three days. And the tumor site of each nude was irradiated by a 660 nm laser with a fluence rate of 0.1 W cm⁻² for 10 min at 12 h after materials injection. Meanwhile the body weights and tumor volumes were recorded for further analysis till day 14. The volumes of the tumors were calculated according to the equation: $V (\text{mm}^3) = 0.5 \times \text{length} \times \text{width}^2$.

3. Results and Discussion

3.1. The Preparation and Evaluation of Cas9-Chl@F127

Metal ions, as cofactors of enzymes can greatly improve the catalytic activity of enzymes, but there are only a few biomaterials developed taking advantage of interaction of metal ions and Cas9.^[36–38] Given the abundance of Mg naturally existing in green plants, we set out to explore the relationship of Mg²⁺ and Cas9 by treating Cas9 with different concentrations of Mg²⁺, following examining the cleavage of target DNA fragments. As showed in **Figure 1a,b**, we selected a low concentration of Cas9 so that the target gene (see method for the sequence) was not cleaved at this concentration. In contrast, in the presence of increasing concentrations of Mg²⁺, the endonuclease activity of Cas9 was greatly enhanced in a dose-response manner, suggesting that Mg²⁺ can act as an enzyme cofactor to augment the catalytic activity of Cas9. According to some theoretical studies, Mg²⁺ enables the phosphodiester bonds of DNA to be cleaved more easily by altering Cas9 nucleophilicity.^[34,35] We

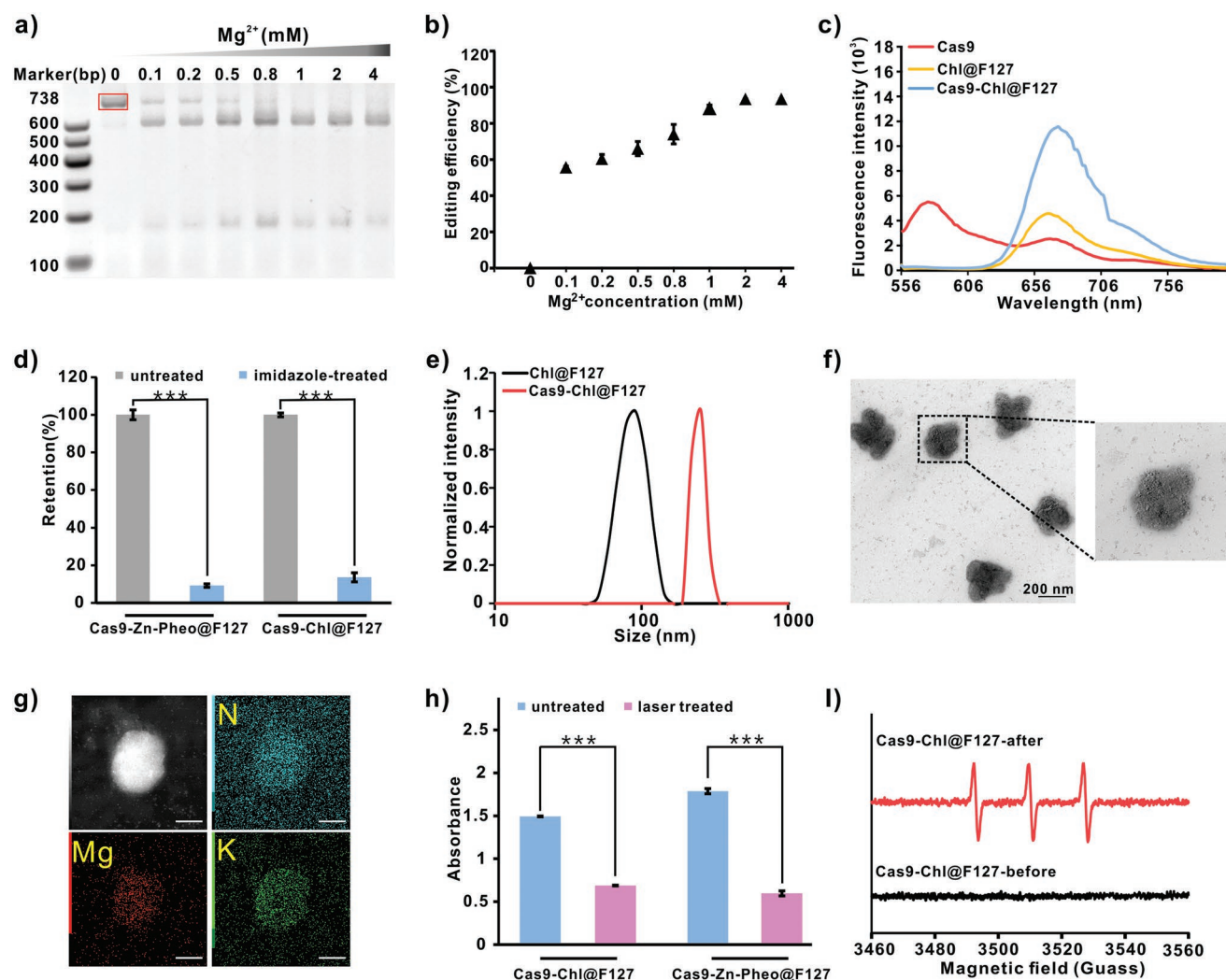


Figure 1. Characterization of Cas9-Chl@F127 micelles. a) Agarose gel electrophoresis of target gene before and after cleavage by Cas9 in the presence of different concentrations of Mg^{2+} , and b) gene editing efficiency of Cas9 in the presence of different Mg^{2+} concentrations, calculated by the intensity of band at 738 bp normalized to the band intensity in the lane without Mg^{2+} highlighted in a red box. c) Fluorescence spectra of Cas9, Chl@F127, and Cas9-Chl@F127. Cas9 and Chl were labeled with Cy3 and Cy5, respectively. d) Fluorescence intensity of Cas9-FITC-Zn-Pheo@F127 and Cas9-FITC-Chl@F127 before and after treatment by 500 mM imidazole. e) Size distribution measured by dynamic light scattering (DLS). f) TEM images (scale bar: 200 nm) and g) the corresponding elemental mapping of Cas9-Chl@F127, scale bar: 100 nm. h) UV-VIS absorption spectra of Cas9-Zn-Pheo@F127 and Cas9-Chl@F127 before and after treated by a 1,3-diphenylisobenzofuran (DPBF). i) ESR spectra of Cas9-Chl@F127 under laser irradiation. Significance was analyzed by one-way ANOVA with Bonferroni's post hoc test. ** $p < 0.01$, *** $p < 0.001$, and **** $p < 0.0001$.

also examined other metals including Mn^{2+} , Zn^{2+} , Ni^{2+} , Cu^{2+} , Fe^{2+} , Co^{2+} and Ca^{2+} , and found that, compared with Mg^{2+} , these metal ions, at least in the experimental concentrations, have weak or no enhancement effect for Cas9 gene-editing activity (Figure S1, Supporting Information).

Chlorophyll a (Chl) was extracted from chlorella and Mg in the center of Chl can be de-chelated in the acidic condition, affording pheophytin (Pheo). Mass spectrum were used to verify the presence of Chl and Pheo, as shown in Figure S2, Supporting Information. Hydrophobic Chl and Pheo could be encapsulated in Pluronic F127 (F127) micelles via hydrophobic interaction, forming Chl@F127 and Pheo@F127, respectively.^[39] Histidine (His)-tagged Cas9 could be chelated to Chl@F127 via coordination of Histidine and Mg^{2+} (Scheme 1). Zn^{2+} was post-labelled in the center of Pheo after encapsulation

in F127 micelles and the resulting Pheo-Zn@F127 was used as a control. In order to verify the coordination of Mg^{2+} and His-tagged Cas9, Cyanine 3 (Cy3) and Cyanine 5 (Cy5) were labelled on Cas9 and amine-modified F127, respectively. After admixing Cy3-labelled Cas9 and Cy5-labelled Chl@F127, the fluorescence of Cy5 was significantly enhanced at the Cy3 excitation wavelength, owing to fluorescence resonance emission transfer (FRET), suggesting successful chelation of Cas9 onto micelles (Figure 1c). The chelation strategy was also applied for Cas9-Zn-Pheo@F127, verified by a similar fluorescence resonance emission transfer (FRET) assay (Figure S3a, Supporting Information). Furthermore, we next labelled Cas9 with FITC and the fluorescence of Cas9-Chl@F127 and Cas9-Zn-Pheo@F127 decreased after treatment by 500 mM imidazole following removal of free FITC-labelled Cas9 by ultrafiltration, which also

validates successful chelation of Mg^{2+} and Cas9, given the competition coordination of imidazole with Mg^{2+} (Figure 1d).

After Cas9 chelation, the average size of Cas9-Chl@F127 increased from 91 (Chl@F127) to 255 nm (Cas9-Chl@F127) (Figure 1e), and the size of Cas9-Zn-Pheo@F127 also increased to 255 nm (Figure S3b, Supporting Information). The transmission electron microscopic (TEM) and scanning electron microscopic (SEM) images of Cas9-Chl@F127 are shown in Figure 1f and Figure S5, Supporting Information. The corresponding elemental mapping reveals that Cas9-Chl@F127 contains Mg element (from chlorophyll), N and K elements (from Cas9 protein) in Figure 1g. The physiological stability was assessed by incubation in 10% v/v fetal bovine serum (FBS) and phosphate buffered solution (PBS) and it was shown that the retention of Cas9 was still over 80% after 12 h (Figure S6, Supporting Information). Next, the ROS generation by Cas9-Chl@F127 and Cas9-Zn-Pheo@F127 was evaluated using 1,3-diphenylisobenzofuran (DPBF) as a probe since the absorbance of DPBF decreases in the presence of ROS. As shown in Figure 1h, after 660 nm laser treatment, Cas9-Chl@F127 and Cas9-Zn-Pheo@F127 induced decrease of DPBF absorbance. For the analysis of electron spin resonance ESR (electron spin resonance), Cas9-Chl@F127 and Cas9-Zn-Pheo@F127 also showed obvious signal after laser treatment, suggesting the successful generation of ROS by these nanoparticles (Figure 1i and Figure S7, Supporting Information).

3.2. The ATP and pH Responsive Release of Cas9

Intracellular Cas9 release in a controlled manner is highly preferred because it facilitates Cas9 to enter nucleus and avoid

off-target effect. Mg could be de-chelated from Chl@F127 in an acidic condition due to protonated pyrrole nitrogen of Chl.^[39,40] When the pH was 3, 4, 5 and 6, the absorbance spectra of Chl@F127 altered as shown in Figure S8a, Supporting Information. The color of Chl@F127 changed from bright green to yellowish green (Figure S8b, Supporting Information). New spots on thin layer chromatography are observed in Figure S8c, Supporting Information. Similarly, endogenously existing adenosine triphosphate (ATP), competing with Histidine and also binding with metal ions, could result in the de-chelation of Mg^{2+} from chlorophyll as shown in Figure S9, Supporting Information.^[41-43] Next, the Cas9 release profile from Cas9-Chl@F127 was investigated in a simulated tumor microenvironment with acidic or abundant ATP conditions using FITC-labelled Cas9, following dialysis to remove free Cas9 released from metal coordination micelles. In addition to the de-chelation of Mg^{2+} from chlorophyll leads to Cas9 release, the protonation of the histidine in intracellular acidic microenvironments also disrupts metallo-coordinated interactions of Mg^{2+} and histidine-labeled Cas9, resulting in the release of Cas9.^[44,45] As shown in Figure 2a, Cas9 could be released over 93% after 4.5 h at pH = 5.5, but not at pH = 7.4. And about 98% Cas9 could also be released within 4 h in the presence of 10 mM ATP (Figure 2b). The release reached over 91% within 2 h in the presence of both 10 mM and pH = 5.5, suggesting that the release rate of Cas9 was doubled compared with single stimulus (Figure 2c). The average size of Cas9-Chl@F127 also decreased from 164 to 50 nm after treatment by 10 mM ATP or/and pH = 5.5, demonstrating the acid and ATP responsive release profile of Cas9-Chl@F127 in tumors (Figure 2d). Sodium dodecyl sulfate polyacrylamide gel

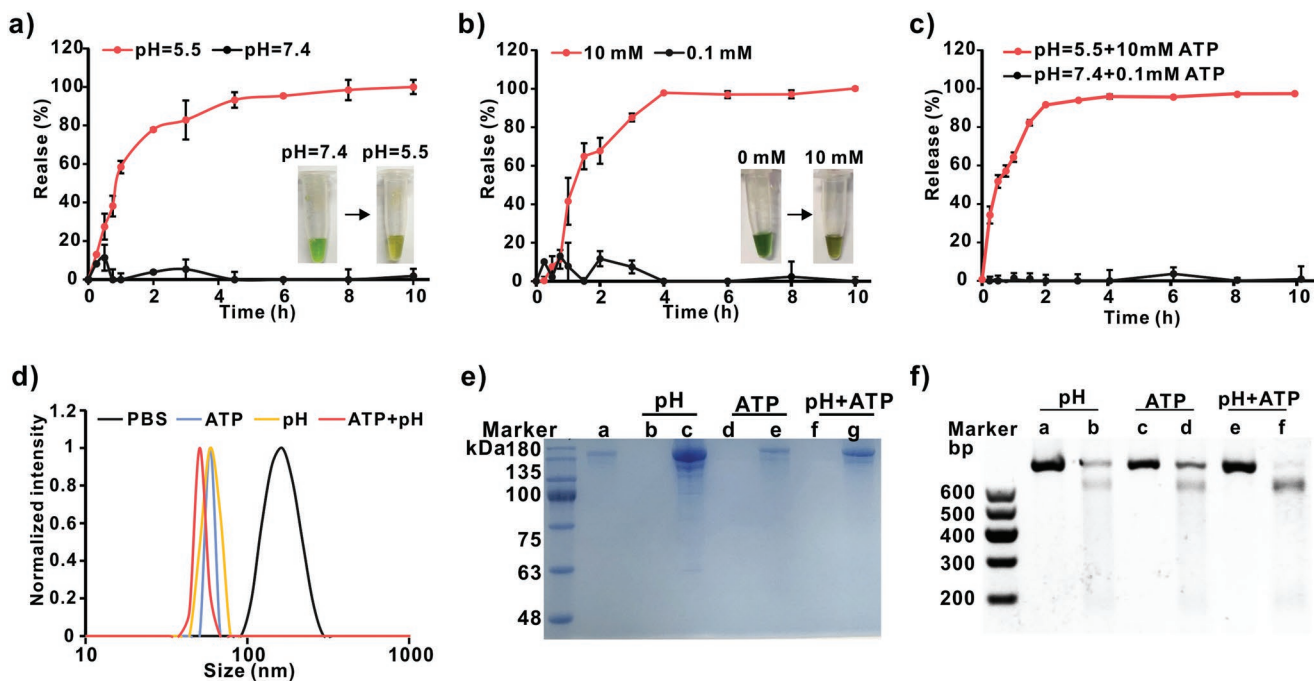


Figure 2. Triggered release of Cas9 by the acidic condition or ATP. The a) pH, b) ATP, and c) pH+ATP dependent release kinetics of Cas9 from different formulations as indicated. d) DLS measurements of Cas9-Chl@F127 after treatment by pH = 5.5, 10 mM ATP, and pH = 5.5+10 mM ATP. e) SDS-PAGE analysis of protein before and after Cas9-Chl@F127 was treated by pH = 5.5, 10 mM ATP and pH = 5.5+10 mM ATP. f) Gene editing effect of the released Cas9 determined by agarose gel electrophoresis, a) pH = 7.4; b) pH = 5.5; c) 0.1 mM ATP; d) 10 mM ATP; e) pH = 7.4+0.1 mM ATP; f) pH = 5.5+10 mM ATP.

electrophoresis (SDS-PAGE) was also used to identify the presence of free Cas9 after low pH and ATP treatment. As shown in Figure 2e, only after incubation with 10 mM ATP or/and pH = 5.5, the protein band with a molecular weight of about 150 kDa could be observed, indicative of the release of free Cas9. And the Cas9 released from Cas9-Chl@F127 preserved its catalytic activity of cleaving DNA fragments but Cas9 in Cas9-Chl@F127 form did not exhibit catalytic activity (Figure 2f).

3.3. The Intracellular PDT and Gene-Editing Effect of Cas9-Chl@F127

Then we investigated cellular uptake of Cas9-Chl@F127 micelle and intracellular release behavior. Figure S10, Supporting Information, shows that FITC-labelled Cas9-Chl@F127 micelles could be successfully taken up by A549 cells and

the fluorescence reached a plateau at about 8 h. As shown in Figure 3a and Figure S11, Supporting Information, green fluorescence of FITC-labelled Cas9-Chl@F127 was not completely overlapped with the red fluorescence from lysosomes tracker, indicating that Cas9 could escape from the lysosome and enter the cytoplasm, probably because Mg^{2+} could be de-chelated from Cas9-Chl@F127 in acidic conditions and ATP-rich environment and interacted with negatively charged membrane, but further in-depth studies are needed for the mechanism. The endocytosis pathways were also investigated by adding caveolae-dependent endocytosis inhibitor (*M β CD*), micropinocytosis-mediated endocytosis inhibitor (amiloride) or at low temperature. The uptake of FITC-labeled Cas9 was significantly reduced in the presence of methyl- β -cyclodextrin (*M β CD*), demonstrating that Cas9-Chl@F127 micelles enter cells mainly through caveolae-dependent endocytosis (Figure S12, Supporting Information). We also found that the intracellular Mg^{2+}

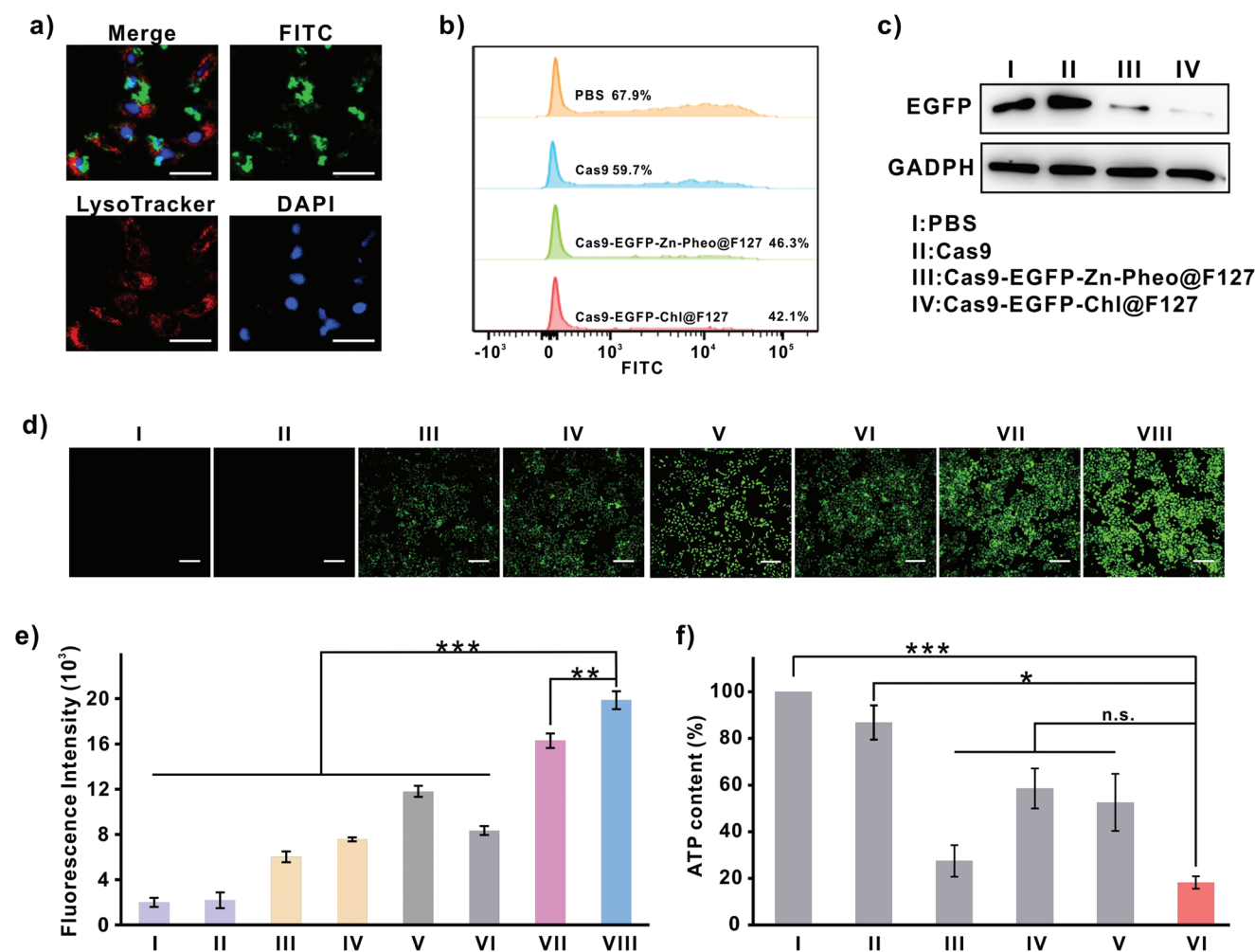


Figure 3. Intracellular gene editing and ROS generation of Cas9-Chl@F127. a) Intracellular localization and lysosome escape of Cas9-FITC-Chl@F127 in A549 cells, scale bar: 50 μ m. b,c) Flow cytometric assay and western blot of EGFP-expressed A549 after treatment by free Cas9, Cas9-Zn-Pheo@F127, and Cas9-Chl@F127. d) Images and e) quantification of ROS level investigated by the fluorescence probe of DCFH-DA after treatment by different samples including I) PBS; II) Cas9; III) Pheo@F127; IV) Chl@F127; V) Cas9-APE1-Chl@F127; VI) Cas9-NRF2-Chl@F127; VII) Cas9-APE1-NRF2-Zn-Pheo@F127; VIII) Cas9-APE1-NRF2-Chl@F127. f) ATP content of A549 cells treated by different samples including I) PBS; II) Cas9; III) Cas9-APE1-Chl@F127; IV) Cas9-NRF2-Chl@F127; V) Cas9-APE1-NRF2-Zn-Pheo@F127; VI) Cas9-APE1-NRF2-Chl@F127. Significance was analyzed by one-way ANOVA with Bonferroni's post hoc test. ** $p < 0.01$, *** $p < 0.001$, and **** $p < 0.0001$.

concentration in A549 cells increased by about eightfold after the uptake of Cas9-Chl@F127 micelles, which could potentially augment the gene-editing performance of Cas9 (Figure S13, Supporting Information). Since the anti-cancer efficacy of Cas9-Chl@F127 depends on gene editing and ROS generation, the gene editing ability were first evaluated as in Figure 3b,c and Figure S14, Supporting Information. A549 cells expressing enhanced green fluorescent protein (A549-EGFP) was treated by free Cas9, Cas9-Chl@F127, Cas9-Zn-Pheo@F127 and the fluorescence measured by flow cytometry was decreased by 60%, 46% and 42%, respectively. Thus, the gene editing efficacy (calculated by fluorescence decrease percentage normalized to the PBS group) of free Cas9, Cas9-Zn-Pheo@F127 and Cas9-Chl@F127 micelles was calculated to be about 12%, 32% and 38%, respectively. The expressed enhanced green fluorescent protein (EGFP) protein was also evaluated by western blot analysis (Figure 3c). Cas9-Chl@F127 micelles significantly led to the weakest fluorescence signal of EGFP-expressing A549 cells. The higher gene silencing efficiency of Cas9-Chl@F127 is likely ascribed to the Mg^{2+} in Cas9-Chl@F127 micelles that acts as an enzyme cofactor to augment the gene editing behavior of Cas9. The capability of cellular ROS generation was next assessed using 2',7'-dichlorodihydrofluorescein diacetate (DCFH-DA) as a fluorescent probe. As shown in Figure 3d and Figure S15, Supporting Information, the strongest green fluorescence signal was observed in the Cas9-Chl@F127 group, indicating that Cas9-Chl@F127 produced most ROS compared with others.

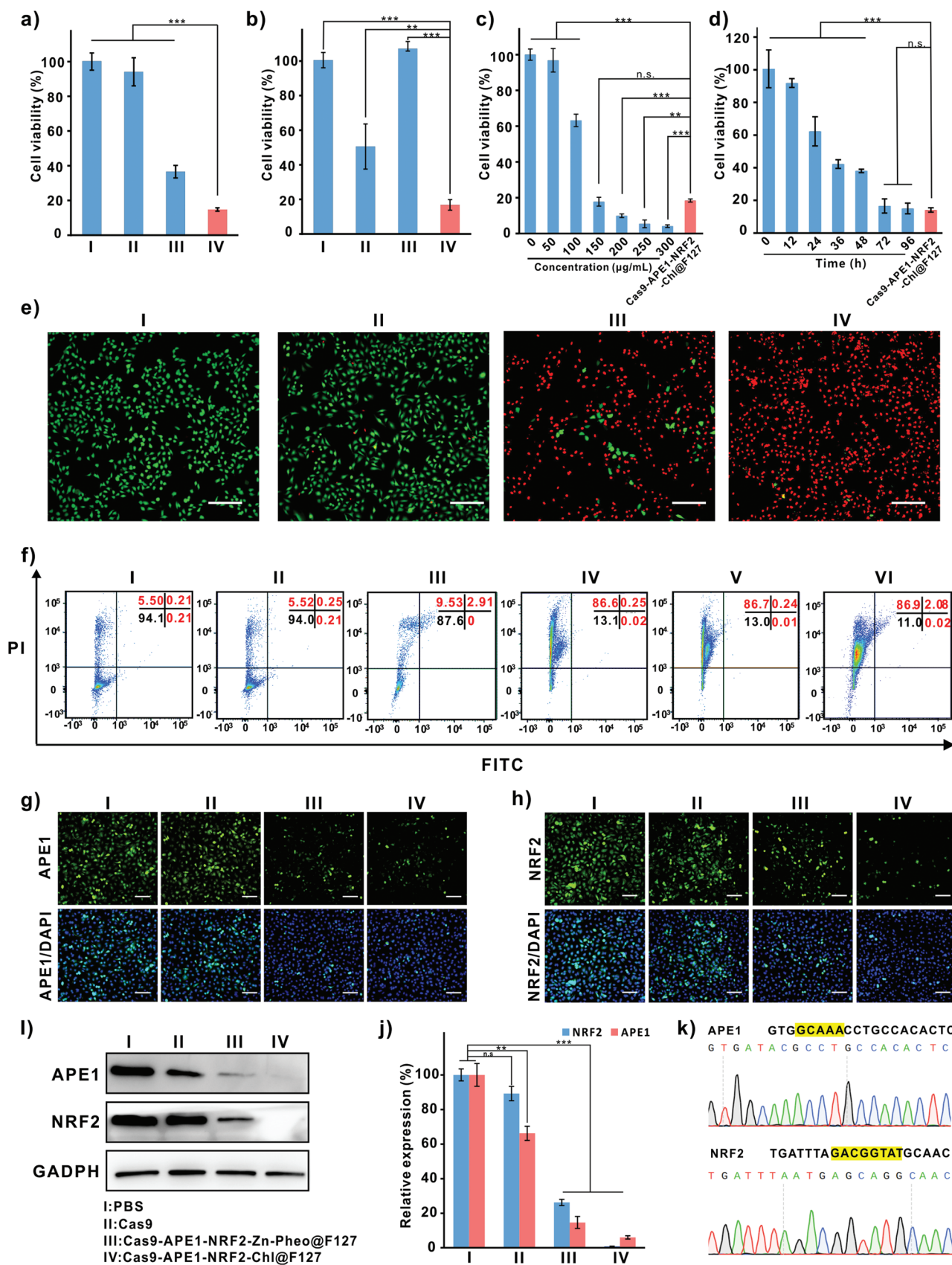
Previous studies have shown that reduced expression of APE1 can impair respiration, resulting in increased intracellular oxygen content and enhanced photodynamic effect. Also, functional macromolecules such as proteins and DNA can be oxidized by ROS, but the intracellular oxidoreductase NRF2, as a defense mechanism, can repair the damage by mitigating the destructive effect of ROS to cancer cells. Therefore, in this study we employed two guide RNAs to cut out the genes of APE1 and NRF2 mediated by Cas9 system, giving rise to enhanced anti-cancer efficacy. The combination of the two pathways significantly increased the level of ROS compared to each single one, as shown in Figure 3d,e. Cas9-Chl@F127-treated cells remarkably reduced ATP level compared with PBS group, indicating that Cas9 successfully interfered with the function of mitochondrial as the main location for ATP generation (Figure 3f). Moreover, Cas9-APE1-NRF2-Zn-Pheo@F127 micelles can also generate ROS and reduce ATP, but the effect is not as pronounced as that of Cas9-APE1-NRF2-Chl@F127, reflecting that Mg^{2+} acts as a cofactor to augment the gene-editing of Cas9.

3.4. The Efficacy of Cas9-Chl@F127 on Killing A549 Tumor Cells

The anti-tumor therapeutic efficacy of Cas9-Chl@F127 micelles was then assessed. The cytotoxicity of Cas9-Chl@F127 to NIH-3T3 and human embryonic kidney (HEK-293) cells was first investigated. No noticeable toxicity of Cas9-Chl@F127 to normal cells was observed as shown in Figure S16, Supporting Information. However, the cell viability of A549 cells after co-culture with Cas9-APE1-NRF2-Chl@F127 is only 14%, compared with the PBS treatment (Figure 4a), indicating that

chlorophyll-mediated photodynamic therapy and Cas9-mediated gene editing therapy have a potent synergistic killing effect on tumor cells because of the introduction of Mg^{2+} . The cell viability of Cas9-APE1-NRF2-Zn-Pheo@F127 micelles was 36%, which was slightly higher than that of Cas9-APE1-NRF2-Chl@F127 micelles, suggesting that Mg^{2+} enhanced the endonuclease behavior of Cas9 (Figure 4a). The gene cutting efficiency by double sgRNAs (16%) was higher than that of single sgRNA (Figure 4b). Phototoxicity is a serious potential side effect of PDT, and therefore reducing the dosage of photosensitizers and laser irradiation time are effective approaches to overcome the phototoxicity problem. In Figure 4c, different concentrations of Chl@F127 were used as PDT paradigm alone and $50 \mu\text{g mL}^{-1}$ Cas9-APE1-NRF2-Chl@F127+laser was used as the synergistic combination therapy. The combination of gene editing and photodynamic therapy could lower the dosage of photosensitizers by 3 times (Figure 4c). Moreover, PDT could shorten the treatment duration of the single gene therapy. Previously we reported that A549 cells could also be killed by cutting the genes of polo-like kinase 1 (PLK-1) and we used this paradigm as a control of single gene therapy using Cas9-PLK1-Chl@F127^[45,46] As shown in Figure 4d, the synergistic therapeutic treatment time was decreased by 48 h compared with the sole gene editing therapy. The therapeutic killing effect by Cas9-APE1-NRF2-Chl@F127 for 24 h was similar to that of Cas9-PLK1-Chl@F127 micelles treated for 72 h, indicative of the advantage of shortened treatment time. Live/dead staining results showed that treatment by Cas9-APE1-NRF2-Chl@F127 induced significant apoptosis, displaying red fluorescence signal in Figure 4e and Figure S17, Supporting Information, in consistency with the results in Figure 4a. Apoptosis assay showed that Cas9-NRF2-Chl@F127, Cas9-APE1-Chl@F127, Cas9-APE1-NRF2-Zn-Pheo@F127 and Cas9-APE1-NRF2-Chl@F127 micelles caused 7%, 86%, 86% and 88% apoptosis rate compared with the PBS group (Figure 4f), Cas9-APE1-NRF2-Chl@F127 led to the strongest apoptosis rate. In conclusion, the synergistic therapy of chlorophyll-mediated photodynamic therapy and Cas9-mediated gene editing has an excellent anti-tumor performance on A549 tumor cells.

Next, the expression levels of intracellular targeted proteins were evaluated to assess the gene-editing performance. Immunofluorescence analysis showed that the fluorescence signals of APE1 and NRF2 proteins in cells treated by Cas9-APE1-NRF2-Chl@F127 became weaker, suggesting that Cas9 successfully interfered with the expression of APE1 and NRF2 (Figure 4g,h). Cas9-APE1-NRF2-Zn-Pheo@F127 also decreased APE1 and NRF2 protein expression, but not as significantly as that of Cas9-APE1-NRF2-Chl@F127 micelles, indicating that Mg^{2+} can augment the gene editing of Cas9. Western blot showed that the APE1 and NRF2 protein in cells treated with Cas9-Chl@F127 micelles were almost invisible, and the APE1 and NRF2 protein contents were only 0.82% and 6%, respectively, compared with the PBS group (Figure 4i,j). Altogether, Cas9-Chl@F127 micelles could decrease the expression of APE1 and NRF2 proteins, and Mg^{2+} could augment the gene cutting efficiency of Cas9. In Sanger sequencing analysis, the change of base sequences near the target sites of APE1 and NRF2 indicates that the genes of APE1 and NRF2 were disrupted by Cas9-APE1-NRF2-Chl@F127 micelles (Figure 4k).



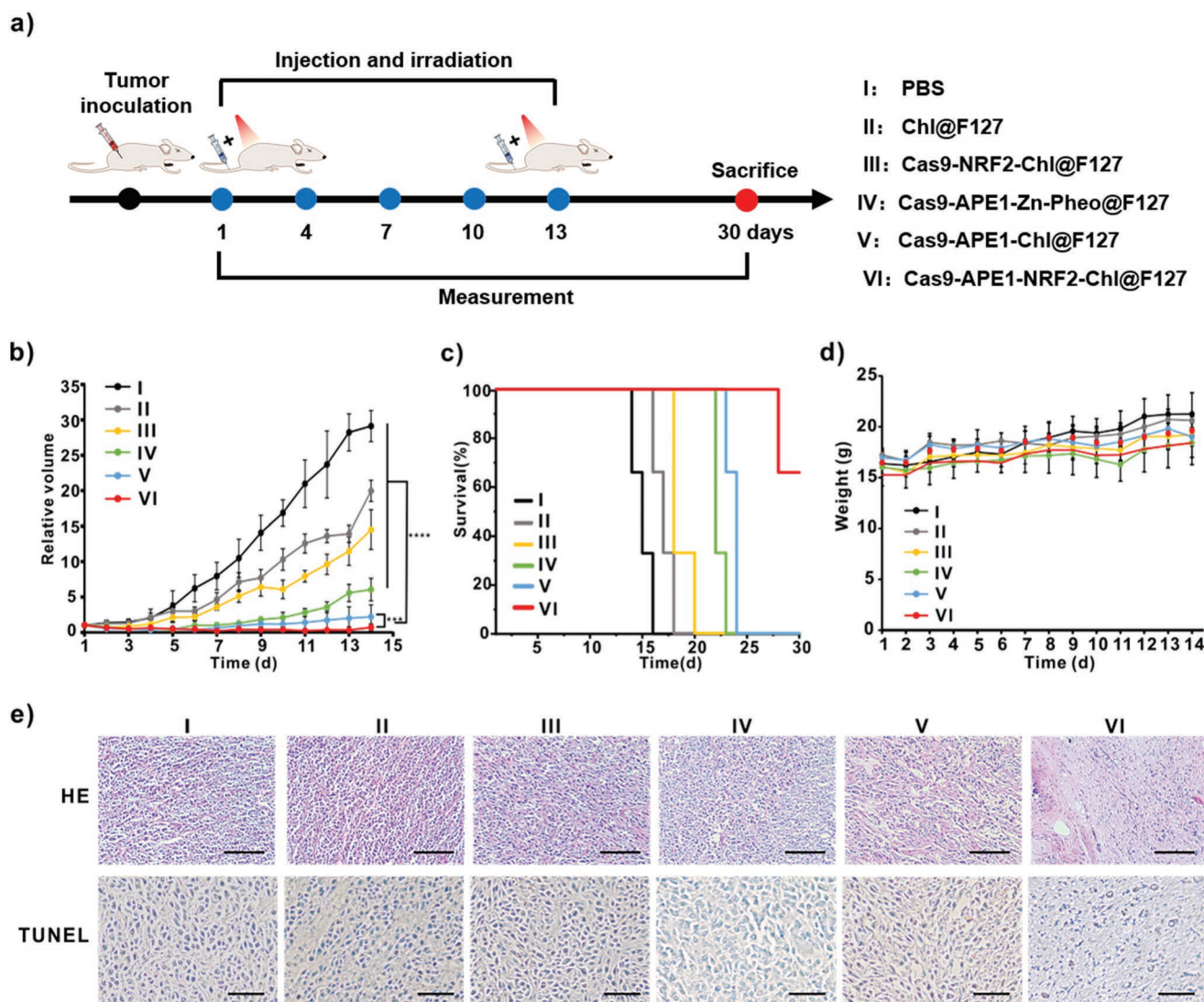


Figure 5. Antitumor effect of Cas9-Chl@F127 in vivo. a) Scheme of therapeutic treatment by Cas9-Chl@F127 and other controls. Injection of different nanoparticles was conducted every three days. I) PBS; II) Chl@F127; III) Cas9-NRF2-Chl@F127; IV) Cas9-APE1-Zn-Pheo@F127; V) Cas9-APE1-Chl@F127; VI) Cas9-APE1-NRF2-Chl@F127. Tumors were irradiated by a 660 nm laser with fluence rates 0.1 W cm^{-2} for 10 min after 12 h since sample injections. b) Tumor growth profiles ($n = 4$); c) survival rate over time ($n = 3$); d) body weight change profiles and e) representative images of H&E staining (scale bar: $100 \mu\text{m}$) and TUNEL staining of tumor tissues (scale bar: $50 \mu\text{m}$) after mice were treated by formulation I to VI. Significance was analyzed by one-way ANOVA with Bonferroni's post hoc test. ** $p < 0.01$, *** $p < 0.001$, and **** $p < 0.0001$.

3.5. Anti-Tumor Efficacy by Cas9-Chl@F127

Encouraged by the results in vitro, we lastly investigated the anti-tumor potency of Cas9-Chl@F127 on an A549 tumor-

bearing mouse model. As demonstrated in Figure 5a, when the size of tumors of nude mice reached 50 mm^3 after tumor cell inoculation, mice were intravenously given different formulations including PBS, Chl@F127, Cas9-NRF2-Chl@F127,

Figure 4. In vitro gene editing of Cas9-APE1-NRF2-Chl@F127 in A549 cells. a) The cell viability of A549 cells treated by PBS (I), Cas9 (II), Cas9-APE1-NRF2-Zn-Pheo@F127 (III), and Cas9-APE1-NRF2-Chl@F127 (IV). b) The cell viability of A549 cells treated by PBS (I), Cas9-APE1-Chl@F127 (II), Cas9-NRF2-Chl@F127 (III), and Cas9-APE1-NRF2-Chl@F127 (IV). c) The cell viability of A549 cells treated by different concentrations of Chl@F127 and $50 \mu\text{g mL}^{-1}$ Cas9-APE1-NRF2-Chl@F127. All groups were treated by laser (660 nm , 0.1 W cm^{-2} for 5 min). d) The cell viability of A549 cells treated by Cas9-PLK1-Chl@F127 as gene editing paradigm alone (no laser treatment) and Cas9-APE1-NRF2-Chl@F127+laser (660 nm , 0.1 W cm^{-2} for 5 min). e) The images of A549 cells treated by samples and costained by PI and calcein AM, scale bar: $200 \mu\text{m}$, I) PBS; II) Cas9; III) Cas9-APE1-NRF2-Zn-Pheo@F127; IV) Cas9-APE1-NRF2-Chl@F127. f) Apoptosis analysis of cells treated with different drug formulations using flow cytometry with Annexin V-FITC/PI assay, I) PBS; II) Cas9; III) Cas9-NRF2-Chl@F127; IV) Cas9-APE1-Chl@F127; V) Cas9-APE1-NRF2-Zn-Pheo@F127; VI) Cas9-APE1-NRF2-Chl@F127. g,h) Immunofluorescence analysis (scale bar: $100 \mu\text{m}$), I) PBS; II) Cas9; III) Cas9-APE1-NRF2-Zn-Pheo@F127; IV) Cas9-APE1-NRF2-Chl@F127. i) Western blotting and j) quantitative analysis of APE1 and NRF2 proteins in A549 cells with different treatments, I) PBS; II) Cas9; III) Cas9-APE1-NRF2-Zn-Pheo@F127; IV) Cas9-APE1-NRF2-Chl@F127. k) Sanger sequence to detect genomic modification of APE1 and NRF2 in A549 cells after treatment with Cas9-APE1-NRF2-Chl@F127. Significance was analyzed by one-way ANOVA with Bonferroni's post hoc test. ** $p < 0.01$, *** $p < 0.001$, and **** $p < 0.0001$.

Cas9-APE1-Zn-Pheo@F127, Cas9-APE1-Chl@F127 and Cas9-APE1-NRF2-Chl@F127 every three days for 4 times, followed by monitoring the tumor size and body weight. After a 14-day treatment, the tumor volume in the Cas9-APE1-NRF2-Chl@F127 decreased from 48 to 36 mm³ (Figure 5b and Figure S20, Supporting Information), while the PBS groups continued increasing to over 1000 mm³, indicating that Cas9-APE1-NRF2-Chl@F127 has a superior antitumor effect. In addition, Mg²⁺ showed a positive effect on enhancing Cas9 gene-editing activity and the tumor volume in the Cas9-APE1-Zn-Pheo@F127 group increased to 343 mm³ within 14 days (Figure 5b). The combination of APE1 and NRF2 sgRNA was also advantageous compared with single sgRNA. The tumor volume in Cas9-NRF2-Chl@F127 and Cas9-APE1-Chl@F127 groups increased to 609 and to 164 mm³, respectively, within 14 days (Figure 5b). Compared with the single treatment groups, some mice treated with Chl@F127 died on day16 (Figure 5c and Figure S18, Supporting Information). And the mice treated by Cas9-APE1-NRF2-Chl@F127 could survive till day 28 whereas mice in PBS group survived for only 14 days (Figure 5c, and Figures S18 and S19, Supporting Information). In addition, no significant change of body weight of mice was observed within 14 days, probably because of the inherent safety of this chlorophyll-based biomaterial (Figure 5d). And aberrant cellular morphology and extensive nuclear shrinkage could be observed in the tumor tissue treated by Cas9-APE1-NRF2-Chl@F127 (Figure 5e). The terminal deoxynucleotidyl transferase-mediated deoxyuridine triphosphate nick end labeling (TUNEL) assays also revealed a different extent of apoptosis among the treatment groups, but the tumor tissues treated by Cas9-APE1-NRF2-Chl@F127 had the most apoptotic cells (Figure 5e). No noticeable inflammation or lesions was observed in major organs, which indicated that Cas9-APE1-NRF2-Chl@F127 micelles induced no overt tissue damage and toxicity (Figure S21, Supporting Information).

4. Conclusion

In summary, we developed a new CRISPR-Cas9 delivery system using naturally existing chlorophyll-based micelles via metal coordination. Magnesium ion is not only used as a bridge to chelate Cas9 and chlorophyll, enabling synergistic therapy of PDT and genome editing, but also acts as a cofactor to significantly increase the catalytic activity of Cas9. After endocytosis of Cas9-Chl@F127 by tumor cells, pristine Cas9 could be released in response to the dual stimuli of ATP and acidic condition, avoiding the degradation by proteases in lysosomes and potential genotoxicity to normal cell and tissue. In addition, Cas9-Chl@F127 micelles effectively generated ROS upon laser irradiation to effectively kill tumor cells. Mediated by two deliberately designed gRNAs, Cas9 enhanced the accumulation of intracellular oxygen by cleaving APE1, and blocked the defense system of tumor cells by cleaving NRF2, resulting in reprogrammed tumor microenvironment and enhanced PDT effect. Taken together, Cas9-Chl@F127 paves a simple and effective pathway for the delivery of Cas9 that warrants potent anti-tumor efficacy by complementing PDT and gene editing.

Supporting Information

Supporting Information is available from the Wiley Online Library or from the author.

Acknowledgements

This work was supported by the National Natural Science Foundation of China (32071384), the National Key Research and Development Program (2021YFC2102300), and Start-up Grant at Tianjin University and One-thousand Young Talent Program of China.

Conflict of Interest

The authors declare no conflict of interest.

Author Contributions

C.Z. and X.W. contributed equally to this work. C.Z. and Y.Z. conceived this project and wrote the paper. C.Z. and X.W. carried out most experiments. G.L. and Z.J. assisted material synthesis. H.R. and J.L. assisted animal experiments. All authors analyzed the data and approved the manuscript.

Data Availability Statement

The data that support the findings of this study are available in the supplementary material of this article.

Keywords

CRISPR-Cas9, enzymatic cofactor, gene therapy, photodynamic therapy, responsive release

Received: November 10, 2022
Revised: December 27, 2022
Published online: January 24, 2023

- [1] Y. Tang, L. Gao, W. Feng, C. Guo, Q. Yang, F. Li, X. C. Le, *Chem. Soc. Rev.* **2021**, *50*, 11844.
- [2] S. Wang, C. Gao, Y. Zheng, L. Yi, J. Lu, X. Huang, J. Cai, P. Zhang, Y. Cui, A. Ke, *Mol. Cancer* **2022**, *21*, 57.
- [3] L. Xu, K. H. Park, L. Zhao, J. Xu, M. El Refaey, Y. Gao, H. Zhu, J. Ma, R. Han, *Mol. Ther.* **2016**, *24*, 564.
- [4] J. Li, J. J. Røise, M. He, R. Das, N. Murthy, *Adv. Drug Delivery Rev.* **2021**, *168*, 99.
- [5] H. Rahimi, M. Salehiabar, J. Charmi, M. Barsbay, M. Ghaffarlou, M. Roohi Razlighi, S. Davaran, R. Khalilov, M. Sugiyama, H. Nosrati, S. Kaboli, H. Danafar, T. J. Webster, *Nano Today* **2020**, *34*, 100895.
- [6] T. Wei, Q. Cheng, L. Farbiak, D. G. Anderson, R. Langer, D. J. Siegwart, *ACS Nano* **2020**, *14*, 9243.
- [7] S. Zhang, J. Shen, D. Li, Y. Cheng, *Theranostics* **2021**, *11*, 614.
- [8] C. Zhuo, J. Zhang, J. H. Lee, J. Jiao, D. Cheng, L. Liu, H. W. Kim, Y. Tao, M. Li, *Signal Transduction Targeted Ther.* **2021**, *6*, 238.
- [9] M. H. Bruhn, B. E. F. de Ávila, M. B. Gastélum, J. Zhao, D. E. R. Herrera, P. Angsantikul, K. V. Gothelf, L. Zhang, J. Wang, *Angew. Chem., Int. Ed.* **2018**, *57*, 2657.

- [10] G. Chen, A. A. Abdeen, Y. Wang, P. K. Shahi, S. Robertson, R. Xie, M. Suzuki, B. R. Pattnaik, K. Saha, S. Gong, *Nat. Nanotechnol.* **2019**, *14*, 974.
- [11] Y. Pan, J. Yang, X. Luan, X. Liu, X. Li, J. Yang, T. Huang, L. Sun, Y. Wang, Y. Lin, Y. Song, *Sci. Adv.* **2019**, *5*, v7199.
- [12] L. Li, Z. Yang, S. Zhu, L. He, W. Fan, W. Tang, J. Zou, Z. Shen, M. Zhang, L. Tang, Y. Dai, G. Niu, S. Hu, X. Chen, *Adv. Mater.* **2019**, *31*, 1901187.
- [13] Y. Pu, H. Yin, C. Dong, H. Xiang, W. Wu, B. Zhou, D. Du, Y. Chen, H. Xu, *Adv. Mater.* **2021**, *33*, 2104641.
- [14] Y. Lyu, C. Yang, X. Lyu, K. Pu, *Small* **2021**, *17*, 2005222.
- [15] L. Chen, Y. Liu, W. Guo, Z. Liu, *Exploration* **2022**, *2*, 20210099.
- [16] M. Zhang, W. Shao, T. Yang, H. Liu, S. Guo, D. Zhao, Y. Weng, X. Liang, Y. Huang, *Adv. Sci.* **2022**, *9*, 2201135.
- [17] M. He, J. Li, H. Han, C. A. Borges, G. Neiman, J. J. Røise, P. Hadaczek, R. Mendonsa, V. R. Holm, R. C. Wilson, K. Bankiewicz, Y. Zhang, C. M. Sadowski, K. Healy, L. W. Riley, N. Murthy, *Chem. Sci.* **2020**, *11*, 8973.
- [18] Z. Chen, F. Liu, Y. Chen, J. Liu, X. Wang, A. T. Chen, G. Deng, H. Zhang, J. Liu, Z. Hong, J. Zhou, *Adv. Funct. Mater.* **2017**, *27*, 1703036.
- [19] Q. Liu, C. Wang, Y. Zheng, Y. Zhao, Y. Wang, J. Hao, X. Zhao, K. Yi, L. Shi, C. Kang, Y. Liu, *Biomaterials* **2020**, *258*, 120275.
- [20] J. Ryu, E. Won, H. A. R. Lee, J. H. Kim, E. Hui, H. P. Kim, T. Yoon, *Biomaterials* **2020**, *232*, 119736.
- [21] K. Lia, M. Lua, X. Xia, Y. Huang, *Chin. Chem. Lett.* **2020**, *32*, 1010.
- [22] R. R. Allison, G. H. Downie, R. Cuenca, X. Hu, C. J. Childs, C. H. Sibata, *Photodiagn. Photodyn. Ther.* **2004**, *1*, 27.
- [23] C. Chen, J. Wang, X. Li, X. Liu, X. Han, *Comb. Chem. High Throughput Screening* **2017**, *20*, 414.
- [24] H. Wang, M. Li, C. M. Lee, S. Chakraborty, H. Kim, G. Bao, K. W. Leong, *Chem. Rev.* **2017**, *117*, 9874.
- [25] Y. A. Aksoy, B. Yang, W. Chen, T. Hung, R. P. Kuchel, N. W. Zammit, S. T. Grey, E. M. Goldys, W. Deng, *ACS Appl. Mater. Interfaces* **2020**, *12*, 52433.
- [26] X. Huang, W. Zhang, Y. Peng, L. Gao, F. Wang, L. Wang, X. Wei, *ACS Nano* **2022**, *16*, 974.
- [27] C. Michiels, C. Tellier, O. Feron, *Biochim. Biophys. Acta* **2016**, *1866*, 76.
- [28] M. Li, J. Shan, D. Wang, Y. He, Q. Zhou, L. Xia, L. Zeng, Z. Li, G. Wang, Z. Yang, *Cancer Sci.* **2012**, *103*, 882.
- [29] A. Barchiesi, V. Bazzani, A. Jabczynska, L. S. Borowski, S. Oeljeklaus, B. Warscheid, A. Chacinska, R. J. Szczesny, C. Vascotto, *J. Mol. Biol.* **2021**, *433*, 167125.
- [30] S. Deng, X. Li, S. Liu, J. Chen, M. Li, S. Y. Chew, K. W. Leong, D. Cheng, *Sci. Adv.* **2020**, *6*, b4005.
- [31] F. Li, Z. Lv, X. Zhang, Y. Dong, X. Ding, Z. Li, S. Li, C. Yao, D. Yang, *Angew. Chem., Int. Ed.* **2021**, *60*, 25557.
- [32] H. Fan, X. Zhang, Y. Lu, *Sci. China Chem.* **2017**, *60*, 591.
- [33] J. Feng, Z. Xu, F. Liu, Y. Zhao, W. Yu, M. Pan, F. Wang, X. Liu, *ACS Nano* **2018**, *12*, 12888.
- [34] L. Casalino, A. Nierzwicki, M. Jinek, G. Palermo, *ACS Catal.* **2020**, *10*, 13596.
- [35] D. Rogolino, M. Carcelli, M. Sechi, N. Neamati, *Coord. Chem. Rev.* **2012**, *256*, 3063.
- [36] Y. Gao, W. Yang, *Science* **2016**, *352*, 1334.
- [37] H. Wang, Y. Chen, H. Wang, X. Liu, X. Zhou, F. Wang, *Angew. Chem., Int. Ed.* **2019**, *58*, 7380.
- [38] C. Liu, Y. Chen, J. Zhao, Y. Wang, Y. Shao, Z. Gu, L. Li, Y. Zhao, *Angew. Chem., Int. Ed.* **2021**, *60*, 14324.
- [39] Y. Zhang, D. Wang, S. Goel, B. Sun, U. Chitgupi, J. Geng, H. Sun, T. E. Barnhart, W. Cai, J. Xia, J. F. Lovell, *Adv. Mater.* **2016**, *28*, 8524.
- [40] X. Huang, K. Nakanishi, N. Berova, *Chirality* **2000**, *12*, 237.
- [41] R. Mo, T. Jiang, R. DiSanto, W. Tai, Z. Gu, *Nat. Commun.* **2014**, *5*, 3364.
- [42] S. Biswas, K. Kinbara, T. Niwa, H. Taguchi, N. Ishii, S. Watanabe, K. Miyata, K. Kataoka, T. Aida, *Nat. Chem.* **2013**, *5*, 613.
- [43] S. Shao, V. Rajendiran, J. F. Lovell, *Coord. Chem. Rev.* **2019**, *379*, 99.
- [44] X. Yao, L. Chen, X. Chen, Z. Xie, J. Ding, C. He, J. Zhang, X. Chen, *Acta Biomater.* **2015**, *25*, 162.
- [45] C. Li, T. Yang, Y. Weng, M. Zhang, D. Zhao, S. Guo, B. Hu, W. Shao, X. Wang, A. Hussain, X. Liang, Y. Huang, *Bioact. Mater.* **2022**, *9*, 590.
- [46] C. Zhang, H. Ren, G. Liu, J. Li, X. Wang, Y. Zhang, *Adv. Healthcare Mater.* **2022**, *11*, 21023.
- [47] D. Moukheiber, U. Chitgupi, K. A. Carter, D. Luo, B. Sun, S. Goel, C. A. Ferreira, J. W. Engle, D. Wang, J. Geng, Y. Zhang, J. Xia, W. Cai, J. F. Lovell, *ACS Appl. Bio Mater.* **2019**, *2*, 544.